**ARTICLE**　　　　　　　　　　　　　　　　　　　　　　　**Open Access**

# Oxygen vacancy-assisted recovery process for increasing electron mobility in *n*-type BaSnO₃ epitaxial thin films

Daseob Yoon[1], Sangbae Yu[1] and Junwoo Son [ID][1]

**Abstract**
The scattering of charge carriers by line defects, i.e., threading dislocations (TDs), severely limits electron mobility in epitaxial semiconductor films grown on dissimilar substrates. The density of TDs needs to be decreased to further enhance electron mobility in lattice-mismatched epitaxial films and heterostructures for application in high-performance electronic devices. Here, we report a strategy for the post-treatment of epitaxial La-doped BaSnO₃ (LBSO) films by delicately controlling the oxygen partial pressure $p(O_2)$, which achieved a significant increase in the room temperature (RT) electron mobility ($\mu_e$) to $\mu_e = 122\,cm^2\,V^{-1}\,s^{-1}$ at a carrier concentration of $1.1 \times 10^{20}\,cm^{-3}$. This mobility enhancement is mostly attributed to an oxygen vacancy-assisted recovery process that reduces the density of TDs by accelerating the movement of dislocations in ionic crystals under a $p(O_2)$-controlled treatment despite an increase in the density of charged point defects. Our finding suggests that accurate control of the interactions between point defects and line defects can reduce dominant carrier scattering by charged dislocations in epitaxial oxide semiconductors that have dissimilar substrates. This method provides alternative approaches to achieving perovskite oxide heterostructures that have high RT $\mu_e$ values.

## Introduction

Heteroepitaxial growth is the epitaxial growth of semiconductor films on dissimilar substrates (e.g., GaN on Al₂O₃); it has been widely used to obtain single-crystal films for electronic and photonic applications mostly because of the limited availability of single-crystal semiconductor substrates with identical lattice parameters for homoepitaxial growth[1,2]. Inevitably, heteroepitaxial layers contain high densities of structural defects; because of the lattice mismatch between films and substrates, most of the defects are threading dislocations (TDs), which cross the epitaxial layers perpendicularly[2,3]. TD cores consist of point defect complexes (e.g., impurities or vacancies) that have abundant dangling bonds, which form deep acceptors with a space-charge double Schottky barrier around

dislocation lines; these acceptor-like negatively charged TDs generate an effective potential field that induces scattering of electrons by Coulombic interactions[4,5]. This "charged TD scattering" severely reduces the number of free charge carriers and thus diminishes electron mobility ($\mu_e$) in epitaxial semiconductor films (e.g., GaAs[4], InN[6], GaN[3,7]). Therefore, the control of charged TD scattering is a key requirement for achieving heteroepitaxial semiconductor films with an electronic grade if homoepitaxy is not available[3,8,9].

Charged TD scattering also significantly affects electronic transport in epitaxial BaSnO₃ (BSO) films, which are new transparent and wide band-gap oxide semiconductors for transparent and power electronics[9–12]. Although La-doped BSO (LBSO) single crystals have excellent an room temperature (RT) $\mu_e$ of ~320 cm² V⁻¹ s⁻¹ at a carrier concentration of $n = 8.0 \times 10^{19}\,cm^{-3}$ and excellent stability, even at high temperatures, heteroepitaxial LBSO films have much lower $\mu_e$ values (at best,

$\sim$70 cm$^2$ V$^{-1}$ s$^{-1}$ by pulsed laser deposition (PLD)[11] and $\sim$124 cm$^2$ V$^{-1}$ s$^{-1}$ by molecular beam epitaxy (MBE)[13] than single crystals[11]. This low $\mu_e$ has been attributed to the abundance of TDs[9] that inevitably form during epitaxial growth due to large lattice mismatch with the substrate, e.g., SrTiO$_3$ or MgO. Therefore, considerable effort has been devoted to decreasing the density of TDs by using substrates with a lattice constant that is similar to or even the same as that of BSO[13–16] or by inserting buffer layers between BSO epilayers and typical substrates[12,17–19] to release the lattice mismatch strain.

In this article, we report a new strategy to increase the $\mu_e$ of LBSO epitaxial films by exploiting a recovery process that is assisted by oxygen vacancies. By delicately adjusting both the oxygen partial pressure $p(O_2)$ and the temperature during thermal treatment of LBSO epitaxial films, the density of TDs and the degree of mosaicity is significantly reduced, so a maximum RT $\mu_e$ value of 122 cm$^2$ V$^{-1}$ s$^{-1}$ at a carrier concentration of $n = 1.1 \times 10^{20}$ cm$^{-3}$ was achieved. This subtle introduction of an oxygen deficiency during post-treatment improves the crystal quality by decreasing the TD density, $N_{TD}$, which leads to an increase in mobility with a minimal increase in the number of oxygen vacancies as impurity scattering centers. This new strategy that exploits the interactions between point and line defects can be used to further reduce $N_{TD}$ in heteroepitaxial thin films by using oxygen vacancies to lubricate TDs.

## Materials and methods

### Synthesis of epitaxial LBSO thin films

Epitaxial La-doped BaSnO$_3$ (LBSO) thin films with a La-doping content of 0–5% and a thickness of $\sim$100 nm were grown on (001)-oriented SrTiO$_3$(001) and MgO single-crystal substrates by using PLD with a KrF excimer laser in a chamber with an $\sim 10^{-6}$ Torr base pressure. The La-doping ratio was controlled by using targets with different La contents; the targets were synthesized by a conventional solid-solution reaction. A KrF excimer laser ($\lambda = 248$ nm, $\tau = 20$ ns, Compex Pro 102F, Coherent Inc., Santa Clara, CA) was focused on rotating targets at a fluence of $\sim$1.1 J/cm$^2$ and a repetition rate of 10 Hz. The as-grown LBSO layers were grown in a $p(O_2)$ of 260 mTorr at 750 °C to optimize the structural and electrical properties of the as-grown LBSO films.

### $p(O_2)$ control of LBSO thin films during annealing

The degree of oxygen deficiency in the LBSO films was controlled by adjusting either the $p(O_2)$ or the temperature post treatment. The $p(O_2)$ post treatment was controlled by simultaneously applying pure Ar gas and 5% forming gas (Ar containing 5% H$_2$) and changing the flow ratio while maintaining a total flow rate of 500 sccm (Fig. S3). To further suppress the reducing ability of H$_2$

gas to achieve subtle control of the $p(O_2)$, wet H$_2$ was used by passing H$_2$ gas through a Drechsel bottle that contained water. The H$_2$O ratio in the flowing gas was estimated to be $\sim$3% from the water vapor pressure at RT, i.e., 3.17 kPa at 25 °C. A Yttria-stabilized Zirconia (YSZ) sensor accurately measured log $p(O_2)$ as $-3.91$ in a flow of pure Ar gas, $-20.0$ in 5% H$_2$ mixed with Ar at 650 °C, and $-16.6$ in 0.5% wet H$_2$ mixed with Ar at 950 °C. The YSZ sensor measured the voltage difference between the inside of a YSZ cell that was exposed to air and the outside of the same cell that was exposed to flow gas. The measured voltage difference was converted to the $p(O_2)$ in the flow gas by using the Nernst equation[20]:

$$E = \left(\frac{RT}{4F}\right) \log\left(\frac{pO_2(\text{air})}{pO_2(\text{flow gas})}\right),$$

where $E$ (mV) is the electromotive force, $R = 8.3145$ (J mol$^{-1}$ K$^{-1}$) is the universal gas constant, $T$ (K) is the YSZ cell temperature, $F = 96485$ (C/mol) is the Faraday constant, $pO_2(\text{air}) = 0.21$ (bar) is the oxygen partial pressure of air, and $pO_2(\text{flow gas})$ is the oxygen partial pressure of flow gas.

### Materials characterization

The crystallinity of the films was characterized using high-resolution X-ray diffraction (HRXRD, Bruker D8 Discovery X-ray diffractometer) with Cu K$_{\alpha 1}$ radiation ($\lambda = 1.5406$ Å) for $\theta$–$2\theta$ scan, rocking curve (RC) scan, and reciprocal space mapping (RSM). The surface morphology of the films was observed using an atomic force microscope (AFM, VEECO Dimension 3100). Etching-pit analysis was performed by etching the thin films in 0.4 wt % nitric acid for 10 min before their surface morphologies were observed using AFM. Oxygen 1s X-ray photoemission spectroscopy (XPS) was performed with a synchrotron source in an ultrahigh vacuum chamber (base pressure of the analysis chamber $\sim 5.3 \times 10^{-10}$ Torr) at the 4D PES beamline at PLS-II of the Pohang Accelerator Laboratory, Pohang, South Korea, to quantify the oxygen deficiencies before and after H$_2$ treatment. The ratio of oxygen vacancies to lattice oxygens was estimated by the areal ratio of the O(II) peak ($\sim$531.6 eV) to the O(I) peak (530.1 eV). As a binding energy reference, the Au 4f$^{7/2}$ peak was set at 84.0 eV. Time-of-flight secondary ion mass spectrometry (TOF-SIMS) depth profiles were recorded by negative polarity with Cs$^+$ sputtering at 3 keV–20 nA.

The resistivity $\rho$ and carrier concentration $n$ were obtained as functions of the temperature from RT ($\sim$300 K) to liquid nitrogen temperature ($\sim$80 K) using a Hall measurement system with a 0.56-T perpendicular magnetic field. Measurements were made in the van der Pauw geometry with square samples (5 × 5 mm$^2$) and indium

ohmic contacts ($<1 \times 1$ mm$^2$) in the sample corners. The four-terminal resistances were measured by a 1-mA current. For the Hall measurements, the magnetic field was varied between ±0.56 T. The carrier concentration was calculated as $n = 1/(e \times R_H)$, where $R_H$ is the measured Hall coefficient. The electron mobility was calculated as $\mu_e = R_H/\rho$, where the resistivity ($\rho = R_S \times t$) was determined by the van der Pauw method and is independent of any errors in determining the film thickness.

### Theoretical estimation of the dislocation-limited mobility

The dislocation-limited mobility, $\mu_{e,TD}$, was estimated by varying the TD density in the equation[3]:

$$\mu_{e,TD} = \frac{30\sqrt{2\pi}\varepsilon_0^2\varepsilon_s^2 a^2 (kT)^{\frac{3}{2}}}{N_{TD}e^3 f^2 \lambda_D \sqrt{m_e^*}},$$

where

$$\lambda_D = \left(\frac{\varepsilon_0\varepsilon_s kT}{ne^2}\right)^2.$$

In these equations, $\varepsilon_0 = 8.854 \times 10^{-12}$ (F/m) is the vacuum dielectric constant, $\varepsilon_s = 21$ is the relative dielectric constant[12], $a = 4.116$ (nm) is the lattice constant, $k = 1.381 \times 10^{-23}$ (J/K) is the Boltzmann constant, $T = 300$ (K) is the temperature, $N_{TD}$ (cm$^{-2}$) is the TD density, $e = -1.602 \times 10^{-19}$ (C) is the electron charge, $f = 1$ is the fraction of occupied acceptor centers of each TD, $m_e^* = 0.1731 \times 10^{-31}$ (kg) is the electron effective mass[12], and $n$ (cm$^{-3}$) is the carrier concentration.

## Results and discussion

Epitaxial LBSO ([La] = 0–5%) thin films with a thickness of 100 nm were grown on (001)-oriented SrTiO$_3$ (STO) and MgO substrates by PLD at 750 °C. HRXRD $\theta$–$2\theta$ scans of the as-grown films showed only the (00$l$) reflection; this result indicates that the films had (001) pseudomorphic epitaxy without secondary phases. However, the lattice mismatch of BSO ($a = 0.4116$ nm) is −5.4% with the (001)-oriented STO substrate ($a = 0.3905$ nm) and +2.2% with the (001)-oriented MgO ($a = 0.4212$ nm) substrate; these mismatches cause misfits and TDs to form in the epitaxial LBSO layers. The as-grown 1% LBSO epitaxial films exhibited the parameters $n \sim 5.3 \times 10^{19}$ cm$^{-3}$ and RT $\mu_e \sim 15$ cm$^2$ V$^{-1}$ s$^{-1}$ when grown on STO and $n \sim 4.1 \times 10^{19}$ cm$^{-3}$ and RT $\mu_e \sim 16$ cm$^2$ V$^{-1}$ s$^{-1}$ when grown on MgO (Fig. 1, Fig. S1); these values are comparable to those of other as-grown 1% LBSO epitaxial films produced by PLD ($n \sim 6 \times 10^{19}$ cm$^{-3}$, $\mu_e \sim 20$ cm$^2$ V$^{-1}$ s$^{-1}$)[11,21]. When 1% La dopants are fully activated, $n$ is expected to be $\sim 1.5 \times 10^{20}$ cm$^{-3}$, so the observed value of $n \sim 6 \times 10^{19}$ cm$^{-3}$ indicates that approximately only one-third of the La$^{3+}$ dopants provide conducting electrons. This low yield suggests that the donated electrons are trapped at the TDs.

The $\mu_e$ of the as-grown epitaxial layer was optimized using various post-treatments to tune the oxygen chemical potential of the samples. As an initial attempt, the samples were annealed under inert Ar at 650 or 950 °C. Annealing at 650 °C did not change $n$ or $\mu_e$, but annealing at 950 °C increased $\mu_e$ to $\sim 30$ cm$^2$ V$^{-1}$ s$^{-1}$ at RT with an almost constant $n$; this result is consistent with previous reports that $\mu_e$ can be increased by annealing in inert N$_2$ at 1000 °C[21].

To further modulate the degree of oxygen deficiency during the thermal treatment of as-grown LBSO epitaxial films with large TD densities, the LBSO films were thermally annealed at 650 °C under a reducing atmosphere with 5% H$_2$-mixed forming gas (denoted 5% H$_2$); both $n$ and the RT $\mu_e$ increased ($\mu_e \sim 90$ cm$^2$ V$^{-1}$ s$^{-1}$ at $n \sim 1.2 \times 10^{20}$ cm$^{-3}$). The increase in $n$ under a reducing atmosphere may be related to the introduction of carrier-generating point defects such as oxygen vacancies or interstitial hydrogen[22–24]. Treatment under excessively reducing conditions at high temperature (i.e., 5% H$_2$ at 950 °C) to increase the diffusivity of the point defects led to a significant suppression of the (001) XRD peak and insulating properties of the LBSO epitaxial films; these changes can be attributed to the collapse of the BSO crystal structure due to excessive formation (or incorporation) of oxygen vacancies in BSO (Fig. S2). Therefore, to exploit the high ionic mobility at high temperature without causing the collapse of the BSO crystal structure, the concentration of generated oxygen vacancies should be regulated to maintain the lattice framework during H$_2$ treatment.

To achieve this balance, the $p(O_2)$ was precisely controlled in the following way. By flowing 0.5% H$_2$ gas through a Drechsel bottle that contained water, H$_2$O gas was added to the H$_2$ gas in the furnace (i.e., wet H$_2$) (Fig. S3)[25]. The effects of this experimental setup could be predicted from the following reaction equation:

$$\text{BaSnO}_3(s) + \text{H}_2(g) \rightleftharpoons \text{BaSnO}_{3-\delta}(s) + \text{H}_2\text{O}(g).$$
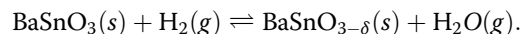
Based on Le Chatelier's principle, both the introduction of H$_2$O and a decrease in the H$_2$ content would suppress the formation of H$_2$O and oxygen vacancies in BaSnO$_3$, even at high temperature. Measurements using an oxygen sensor based on YSZ detected a higher $p(O_2)$ in wet H$_2$ at 950 °C (log $p(O_2) = -16.6$) than in 5% H$_2$ at 650 °C (log $p(O_2) = -20.0$)[20]. This difference confirms that the utilization of wet H$_2$ is an effective method for slightly suppressing the reducing ability at high temperature; this suppression cannot be achieved using 5% H$_2$ alone. With the accurate tuning of the oxygen chemical potential, the wet H$_2$ process at 950 °C gave the maximum RT $\mu_e$ of LBSO ($\sim 122$ cm$^2$ V$^{-1}$ s$^{-1}$ at $n \sim 1.1 \times 10^{20}$ cm$^{-3}$) without collapsing the lattice framework of LBSO, even at high temperature. Therefore, the optimized
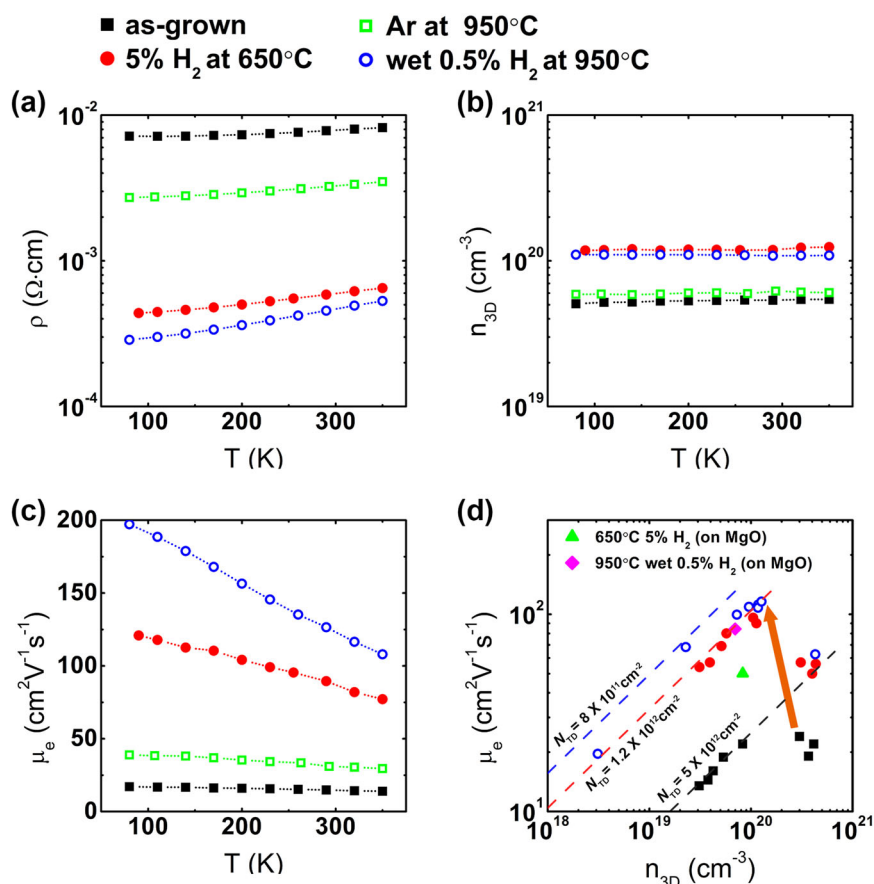
**Fig. 1 Increase in electron mobility of LBSO epitaxial thin films after precise H$_2$ treatment.** Temperature-dependent (**a**) electrical resistivity $\rho$, (**b**) carrier concentration $n$, (**c**) and electron mobility $\mu_e$ of 1% La-doped BaSnO$_3$ thin films: as-grown (black-filled squares), Ar-annealed at 950 °C (green-hollow squares), 5% H$_2$-annealed at 650 °C (red-filled circles), and wet 0.5% H$_2$-annealed at 950 °C (blue-hollow circles). (**d**) $\mu_e$ as a function of $n$ at room temperature (RT) in LBSO films with different La-doping contents: as-grown (black-filled squares), 5% H$_2$-annealed at 650 °C (red-filled circles), and wet 0.5% H$_2$-annealed at 950 °C (blue-hollow circles). Dashed lines: theoretically calculated $\mu_e$ limited by charged-dislocation scattering as a function of threading dislocation density, $N_{TD}$. Note that the RT $\mu_e$ maximum of the H$_2$-treated LBSO films shifts toward the upper left corner and is located near 10$^{20}$ cm$^{-3}$ (orange arrow)

thermal treatment with subtle $p(O_2)$ control could remarkably increase the RT $\mu_e$ in LBSO thin films with a minimal increase in the number of oxygen vacancies as impurity scattering centers. The thermal H$_2$ treatment also increased $\mu_e$ and $n$ in the LBSO epitaxial films on MgO substrates (Fig. S1: $\mu_e$ and $n$ increased from 16 cm$^2$ V$^{-1}$ s$^{-1}$ and 4.1 × 10$^{19}$, respectively, in as-grown LBSO to 76 cm$^2$ V$^{-1}$ s$^{-1}$ and 7.3 × 10$^{19}$ in wet H$_2$ LBSO at 950 °C (50 cm$^2$ V$^{-1}$ s$^{-1}$ and 8.1 × 10$^{19}$ in 5% H$_2$ LBSO at 650 °C) despite the severe crystal mosaicity in LBSO on MgO (Fig. S4); this result indicates that the wet H$_2$ process is very effective for increasing the RT $\mu_e$ regardless of the substrate. To confirm the chemical origin of the point defects and generate more carriers after the H$_2$ treatments, we performed TOF-SIMS and XPS on the as-grown and H$_2$-treated BSO epitaxial films (Fig. S5). The hydrogen anion (H$^-$) signal increased very little after the H$_2$ treatments (Fig. S5a)[26,27], so hydrogen interstitials are

unlikely to be the main origin of mobile carriers. Instead, deconvolution of the O 1s XPS spectra of both films indicates that the areal ratio of the O(II) peak (~531.6 eV) to the O(I) peak (~530.1 eV), which are related to oxygen vacancies and lattice oxygens[23], respectively, increased from 0.588 in as-grown BSO to 1.42 in the 5% H$_2$ BSO films (Fig. S5b, c); this result reveals the formation of oxygen vacancies, which can be additional sources of mobile electrons in the LBSO films after H$_2$ treatment. However, oxygen vacancies usually scatter carriers and thus cannot be the origin of the RT $\mu_e$ increase. Indeed, the formation of oxygen vacancies decreases the RT $\mu_e$ of the LBSO thin film due to increased scattering by the charged point defects[28], which is contrary to our present result in which RT $\mu_e$ increased even with the formation of oxygen vacancies after H$_2$ treatment; this contradiction suggests that a different origin induces the increase in $\mu_e$ after H$_2$ treatment.

To exclude the possibility of electrical conduction through the STO substrate after our precise $H_2$ treatment, the substrate conductance was indirectly estimated from the linear extrapolation of the sheet conductance and (Fig. S6) directly measured with respect to the $H_2$ treatment at different $p(O_2)$ values and temperatures (Fig. S7). Unlike in the typical reducing conditions for producing oxygen-deficient $SrTiO_{3-\delta}$, the STO substrates showed negligible conduction comparable to that of the pristine STO substrate after our delicate thermal treatment (i.e., 5% $H_2$ LBSO at 650 °C and wet $H_2$ LBSO at 950 °C). Therefore, it can be inferred that our mild reducing conditions produced oxygen vacancies in only the LBSO epitaxial layers and are not sufficient to produce oxygen deficiency in the STO substrates. This selective formation of oxygen vacancies in LBSO/STO can be explained by the fact that the formation energy of oxygen vacancies in STO (~3.1 eV)[29] is considerably higher than that in BSO (~1.7 eV)[24].

To gain further insight into electron transport in the LBSO epitaxial films, we measured the temperature dependence of $n$ and $\mu_e$ for 1% La-doped LBSO films treated under different conditions (Fig. 1b, c). $n$ was almost constant with varying temperature in all samples (Fig. 1b), indicating that the films are degenerately doped. In contrast, the temperature dependence of $\mu_e$ was affected by the $p(O_2)$ used during post-treatment (Fig. 1c); this relationship indicates that the dominant carrier scattering mechanism changed. Samples without $H_2$ treatment showed no temperature dependence of $\mu_e$ (e.g., $15\,cm^2\,V^{-1}\,s^{-1}$ at 300 K and $17\,cm^2\,V^{-1}\,s^{-1}$ at 80 K for as-grown LBSO), but those subject to $H_2$ treatment showed a significant increase in $\mu_e$ as the temperature decreased (e.g., $122\,cm^2\,V^{-1}\,s^{-1}$ at 300 K and $197\,cm^2\,V^{-1}\,s^{-1}$ at 80 K for the LBSO film annealed in wet $H_2$ at 950 °C).

To understand the significant increase in $\mu_e$ after the $H_2$ treatment, the resulting $\mu_e$ can be expressed according to Matthiessen's rule[3,12,17]:

$$\mu_e(T)^{-1} = \mu_{e,LO}(T)^{-1} + \mu_{e,CI}(T)^{-1} + \mu_{e,TD}(T)^{-1},$$

where $\mu_{e,LO}$ is $\mu_e$ governed by LO phonon scattering, $\mu_{e,CI}$ is $\mu_e$ governed by charged impurities, and $\mu_{e,TD}$ is $\mu_e$ governed by TDs. The dominant scattering factor changes with $N_{TD}$, as previously reported in the plot of the temperature dependence of $\mu_e(T)$[12,17]: when $N_{TD}$ is high, the contribution of weakly temperature-dependent $\mu_{e,TD}$ is dominant over the contribution of $\mu_{e,LO}$ and $\mu_{e,CI}$, so the resultant $\mu_e$ exhibits negligible change with temperature. However, if $N_{TD}$ is low, $\mu_{e,TD}$ is negligible compared to $\mu_{e,LO}$ and $\mu_{e,CI}$, so the resultant $\mu_e$ shows a strong temperature dependence due to LO phonon-limited scattering, charged-impurity-limited scattering, or both. Our analysis of the dominant scattering mechanisms suggests

that the precise tuning of oxygen vacancies in our LBSO films induces a change in the scattering processes from charged-dislocation-limited scattering to ionized impurity- or LO phonon-limited scattering (or both) by reducing $N_{TD}$.

The change in the dominant scattering mechanism upon $H_2$ treatment can be readily seen in the plot of the RT $\mu_e$ of the LBSO films ([La] = 0–5%) as a function of $n$ at RT (Fig. 1d). Due to competition between charged-dislocation scattering and charged-impurity scattering, the plot of the RT $\mu_e$ vs. $n$ is bell-shaped[3,9,12,17]. In the as-grown and Ar-treated LBSO films, $\mu_e$ was maximized at high $n$ ($\sim5 \times 10^{20}\,cm^{-3}$) and then decreased with decreasing $n$; this relationship demonstrates the strong influence of charged dislocations as charge traps, scattering centers for carriers, or both, and also shows that this influence reduces $n$ and $\mu_e$ simultaneously. After $H_2$ treatment of the LBSO films, both $n$ and $\mu_e$ increased simultaneously in all the LBSO films; this change led to a shift in each data point of $n$ vs. $\mu_e$ toward the upper right corner. This shift indicates that the $H_2$ treatment causes a decrease in the intensity of charge TD scattering despite the increase in the number of charged point defects. In the overall bell-shaped curves, the maximum $\mu_e$ of the $H_2$-treated LBSO films shifted toward the upper left corner (Fig. 1d, orange arrow) and is located near $10^{20}\,cm^{-3}$. In GaN epitaxial films with a high $N_{TD}$, the shift in the maximum $\mu_e$ toward the upper left corner indirectly represents a decrease in $N_{TD}$[3], which again confirms that our subtle $H_2$ treatment reduces $N_{TD}$ and the contribution of charged-dislocation scattering.

As a further check of our model, various X-ray diffraction techniques, e.g., RSM around the (103) Bragg reflection and RC of the (002) reflection, were used to explore the structural origin of the RT $\mu_e$ increase induced by the $p(O_2)$-controlled thermal treatment (Fig. 2). At first glance, the (103) Bragg reflections of the precisely $H_2$-treated LBSO films (Fig. 2c, d) had higher peak intensities and narrower peak widths than those of the as-grown (Fig. 2a) LBSO films (Fig. 2b). Ar treatment of the LBSO films had almost no effect on the full-width half maximum (FWHM) in both the RSM and RC, but both $H_2$ treatments caused significant reductions in the FWHMs in the in-plane direction ($\Delta Q_x$) and the out-of-plane direction ($\Delta Q_z$). In particular, $\Delta Q_x$ decreased considerably more than $\Delta Q_z$ and the RC $\Delta\omega$ in the $H_2$-treated LBSO films (Fig. 2e) (e.g., $\Delta Q_x = 0.0172\,Å^{-1} \rightarrow 0.0111\,Å^{-1}$, $\Delta Q_z = 0.0099\,Å^{-1} \rightarrow 0.0088\,Å^{-1}$, $\Delta\omega = 0.033° \rightarrow 0.026°$ in the wet 0.5% at 950 °C $H_2$ samples). In contrast to the increase in the number of oxygen vacancies in the BSO films after $H_2$ treatment, the distinct narrowing of the RSM (i.e., $\Delta Q_x$) peaks after thermal treatment under a controlled $p(O_2)$ should be related to structural improvement by the reduction in the density of line defects (e.g., $N_{TD}$) in the
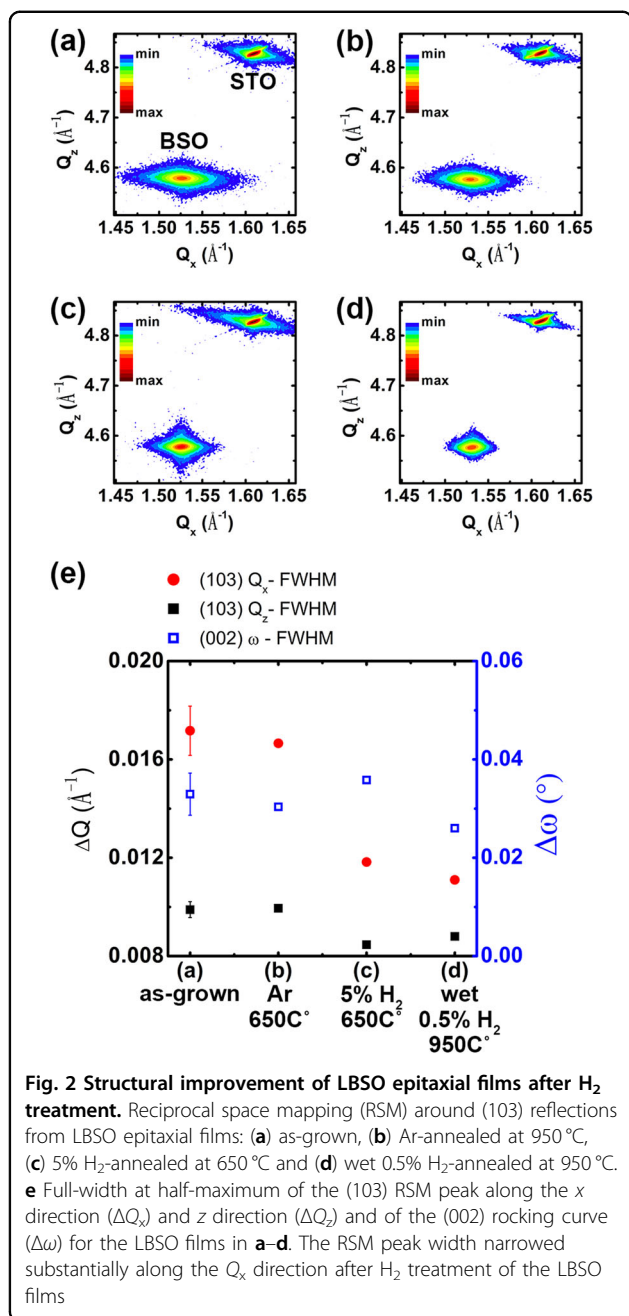
**Fig. 2 Structural improvement of LBSO epitaxial films after H$_2$ treatment.** Reciprocal space mapping (RSM) around (103) reflections from LBSO epitaxial films: (**a**) as-grown, (**b**) Ar-annealed at 950 °C, (**c**) 5% H$_2$-annealed at 650 °C and (**d**) wet 0.5% H$_2$-annealed at 950 °C. **e** Full-width at half-maximum of the (103) RSM peak along the *x* direction ($\Delta Q_x$) and *z* direction ($\Delta Q_z$) and of the (002) rocking curve ($\Delta\omega$) for the LBSO films in **a**–**d**. The RSM peak width narrowed substantially along the $Q_x$ direction after H$_2$ treatment of the LBSO films

where $q$ is a diffraction vector that corresponds to the Bragg reflection plane $(hkl)$[30]. Therefore, if lattice distortion is induced in the in-plane direction $(u_1 = (x, 0, 0))$, then $I(q + \Delta q_x)$ increases but $I(q+\Delta q_z)$ does not, so peak broadening occurs along the $x$ direction. In the case of TDs, in-plane distortion, $u_1$, can be induced by edge-type dislocations but not by screw-type dislocations[30,31]. Therefore, the type of TD in the epitaxial layers affects the direction of lattice distortion, so the RSM FWHMs change asymmetrically. For example, in GaN epitaxial films with a high density of TDs, edge-type TDs widen the in-plane FWHMs and screw-type TDs widen the out-of-plane FWHMs[30–33].

Likewise, the observed reduction in the in-plane FWHMs in our LBSO epitaxial films should be related to a decrease in the edge-type $N_{TD}$ rather than the screw-type $N_{TD}$ after the H$_2$ treatment. Therefore, the H$_2$ atmosphere at high temperature accelerated the elimination of edge-type TDs, which are expected to be the dominant TD type in the as-grown LBSO epitaxial films. Indeed, a Burgers vector of <010>$_a$ was mostly observed in the as-grown LBSO thin films by two-beam dark-field transmission electron microscopy (TEM) imaging (Fig. S8); this observation confirms that edge-type TDs were the dominant TD type. The reduction in $N_{TD}$ after the H$_2$ treatment was confirmed by etching-pit analysis using AFM (Fig. S9). Etching with 0.4% nitric acid creates pits near the cores of the TDs because etching is faster near defective and deformed atomic structures than nearly ordered ones[21,34]. The H$_2$-treated film with a narrow $\Delta Q_x$ had far fewer etching pits than the as-grown film, i.e., $N_{TD}$ was lower in the H$_2$-treated epilayers than in the as-grown epilayers.

The importance of the precise $p(O_2)$ control for inducing the structural improvement responsible for the increases in the RT $\mu_e$ can be demonstrated by the changes in the structural and electrical properties of undoped BSO films after systematically controlling the $p(O_2)$ to change the percentage of H$_2$ gas (0–10 %) at 650 °C during thermal treatment for 1 h (Fig. 3). As the amount of H$_2$ gas increased ($p(O_2)$ decreased) during post-annealing, $\Delta Q_x$ and the RT resistivity of the annealed BSO drastically decreased and almost saturated when the H$_2$ content was 1%; this trend indicates that the improvement in the in-plane structural quality ($\Delta Q_x$), not $\Delta Q_z$, seems to be strongly correlated with the increase in electrical transport. The best structural quality can be observed in the range $0.4 \leq$ H$_2$ content < 1% H$_2$, but an H$_2$ gas content >5% H$_2$ caused $\Delta Q_x$ to increase again; this result confirms that the excessive generation of oxygen vacancies degrades the overall crystal quality. Therefore, simultaneous increases in both the structural and electrical properties require that the $p(O_2)$ be precisely controlled. This conclusion may explain why the RT $\mu_e$ can be

films, which is likely to be the main origin of the increase in the RT $\mu_e$.
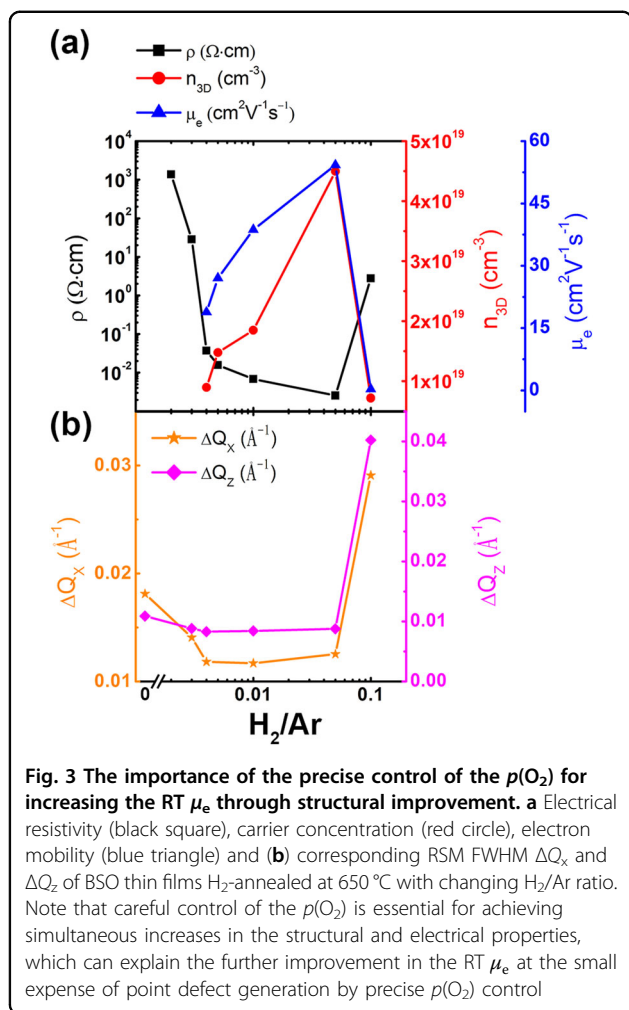
A reduction in $N_{TD}$ for a specific type of TD can explain the reduction in the RSM FWHM in $\Delta Q_x$ after H$_2$ annealing. Dislocations cause local lattice displacement, $u(r)$, which influences the X-ray scattering intensity $I(q)$ as follows:

$$I(q) \propto \left| \int e^{-iq \times u(r)} e^{-iq \times r} dr \right|^2 ,$$

**Fig. 3 The importance of the precise control of the $p(O_2)$ for increasing the RT $\mu_e$ through structural improvement. a** Electrical resistivity (black square), carrier concentration (red circle), electron mobility (blue triangle) and (**b**) corresponding RSM FWHM $\Delta Q_x$ and $\Delta Q_z$ of BSO thin films $H_2$-annealed at 650 °C with changing $H_2$/Ar ratio. Note that careful control of the $p(O_2)$ is essential for achieving simultaneous increases in the structural and electrical properties, which can explain the further improvement in the RT $\mu_e$ at the small expense of point defect generation by precise $p(O_2)$ control

are either in equilibrium or non-equilibrium; the films also contain local deformations near the TD cores due to lattice/thermal mismatch, high-energy growth processes, or both.

Along the dislocation lines, the columns of grown films are slightly tilted or mis-oriented relative to each other, forming mosaic-like structures with local deformation[9]. Once sufficient thermal energy is supplied, the deformation energy can be released in a recovery process that entails dislocation annihilation, thereby reducing $N_{TD}$ and decreasing the lattice distortion induced by the TDs. Because dislocation movement is a prerequisite for dislocation annihilation, point defects such as oxygen vacancies accelerate the movement of dislocations along and across the slip plane, e.g., dislocation climb[35,36]. This climb occurs by the absorption or emission of vacancies, which are thermally activated processes[35], so the rate of climb is directly proportional to the vacancy concentration in ionic crystals. Therefore, dislocation movement that is assisted by oxygen vacancies without creating excessive oxygen deficiencies appears to be very important for improving the structural and electrical properties of the LBSO epitaxial layer by reducing $N_{TD}$. A similar improvement in the structural quality by vacancy-dislocation interaction has been reported in cold-worked
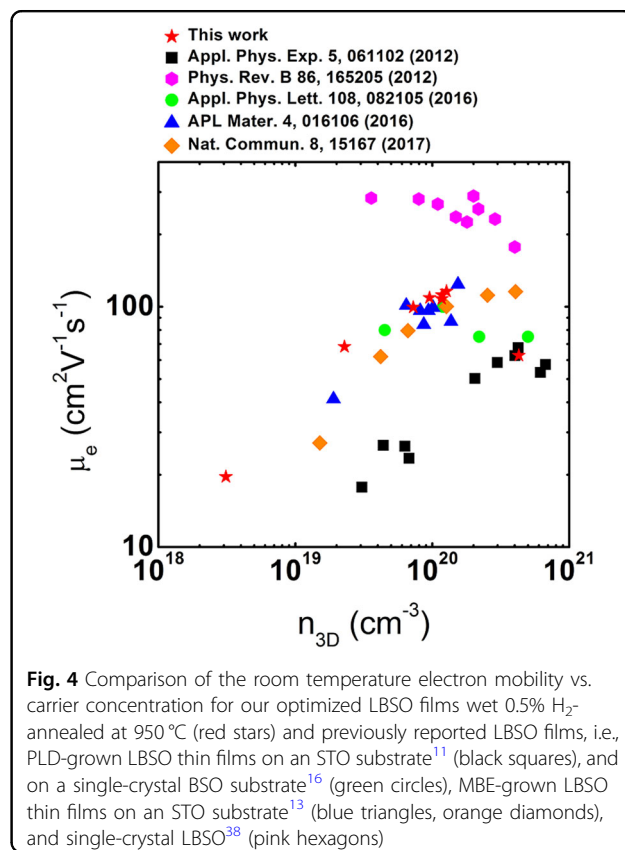
increased using the wet $H_2$ process to slightly improve the precision of the $p(O_2)$ control. If this is the case, the increase in $\mu_e$ after $H_2$ treatment may occur because the improvement imparted by the contribution of $\mu_{TD}$ dominates the degradation caused by the contribution of $\mu_{CI}$.

The electrical and structural results both suggest that the formation of oxygen vacancies by the precise $H_2$ treatment reduces the density of TDs and thereby increases the RT $\mu_e$. Dislocation annihilation assisted by point defects has been traditionally considered an effective recovery process in physical metallurgy[35]: This recovery process is exploited in single-crystal-like materials to release strain energy concentrated around dislocations by removing or rearranging structural defects during the annealing of highly deformed samples at high temperature. The recovery process during heat treatment is kinetically limited by atomic migration, so point defects (e.g., oxygen vacancies in the present study) facilitate dislocation motion and efficiently increase the release of deformed strain[35–37]. In our case, the LBSO epitaxial films grown by PLD contain extended defects, e.g., TDs, which



**Fig. 4** Comparison of the room temperature electron mobility vs. carrier concentration for our optimized LBSO films wet 0.5% $H_2$-annealed at 950 °C (red stars) and previously reported LBSO films, i.e., PLD-grown LBSO thin films on an STO substrate[11] (black squares), and on a single-crystal BSO substrate[16] (green circles), MBE-grown LBSO thin films on an STO substrate[13] (blue triangles, orange diamonds), and single-crystal LBSO[38] (pink hexagons)

Al, in which the presence of vacancies significantly increased the mobility of dislocations[36].

Finally, Fig. 4 shows a comparison of the variation in $\mu_e$ with $n$ at RT for our $H_2$-treated LBSO/STO films with various La concentrations and previously reported LBSO/STO films. With the exception of the bulk LBSO crystals, in which $\mu_e$ increased a relatively small amount as $n$ decreased, all the LBSO films showed bell-shaped curves in the plot of $\mu_e$ vs. $n$ at RT. This curve represents charged-dislocation-limited scattering at low $n$ and ionized impurity scattering at high $n$, at which charge screening at high $n$ suppresses dislocation scattering as a dominant scattering mechanism. The maximal RT $\mu_e$ as a function of $n$ was significantly shifted toward the upper left corner in our wet $H_2$-treated LBSO films compared to the other as-grown LBSO films prepared by PLD. This shift indicates that our precise $H_2$ treatment significantly reduced $N_{TD}$. This reduction in $N_{TD}$ induced by the optimized control of the interactions between point defects and line defects achieves a maximal RT $\mu_e$ in our LBSO (~122 cm$^2$ V$^{-1}$ s$^{-1}$ at ~$n = 1.1 \times 10^{20}$ cm$^{-3}$) that is comparable to the RT $\mu_e$ of other LBSO films whose properties were improved by buffer layers, homoepitaxial growth, or different growth methods (e.g., MBE). However, at a high $n > 10^{20}$ cm$^{-3}$, $\mu_e$ significantly decreased with increasing $n$ in our case, but the LBSO thin films grown by MBE with controlled cation stoichiometry[17] maintained a relatively high RT $\mu_e$ in spite of the increase in $n$ and thus achieved a low resistivity $<10^{-4}$ Ω cm by minimizing the impurity scattering induced by the cation off-stoichiometry. Therefore, a further improvement in the RT $\mu_e$ of our $H_2$-treated LBSO through the precise control of the residual point defects and line defects as scattering centers is possible.

## Conclusion

The precise control of the oxygen partial pressure $p$ $(O_2)$ and temperature during post-treatment with $H_2$ increased $n$ and $\mu_e$ simultaneously in epitaxial La-doped $BaSnO_3$ (LBSO) films and thereby achieved a significant increase in the RT $\mu_e$ (122 cm$^2$ V$^{-1}$ s$^{-1}$ at a carrier concentration of $1.1 \times 10^{20}$ cm$^{-3}$). Despite the possibility that the $H_2$ treatment could increase the number of scattering centers caused by charged point defects (i.e., oxygen vacancies), the precise control of the $p(O_2)$ enabled an increase in the mean free path of electrons in the LBSO thin films. This change is mostly attributed to a reduction in the number of TDs and the mosaicity by the accelerated dislocation movement that occurs due to oxygen vacancy-assisted recovery in ionic crystals. These results suggest that precise control of the interactions between point and line defects can be used to switch the dominant carrier scattering centers in heteroepitaxial oxide films. This strategy using defect chemistry may provide new approaches for achieving perovskite oxide heterostructures that have a high RT $\mu_e$.

## Authors' contributions
J.S. and D.Y. conceived the idea and designed the study. S.Y. and D.Y. performed the film growth and processing, X-ray diffraction studies, transport measurements, AFM observations, and synchrotron measurements. D.Y. and J.S. wrote the manuscript, and all authors commented on it.

## Conflict of interest
The authors declare that they have no conflict of interest.

## References
1. Akasaki, I. Novel Lecture: Fascinated journeys into blue light. *Rev. Mod. Phys.* **87**, 1119 (2015).
2. Kapolnek, D. et al. Structural evolution in epitaxial metalorganic chemical-vapor-deposition grown GaN films on sapphire. *Appl. Phys. Lett.* **67**, 1541–1543 (1995).
3. Ng, H. M., Doppalapudi, D., Moustakas, T. D., Weimann, N. G. & Eastman, L. F. The role of dislocation scattering in n-type GaN films. *Appl. Phys. Lett.* **73**, 821–823 (1998).
4. Wood, J., Howes, M. J. & Morgan, D. V. The effect of dislocations on the electron mobility of GaAs. *Phys. Stat. Sol. (a)* **74**, 493 (1982).
5. You, J. H., L, J.-Q. & Johnson, H. T. Electron scattering due to threading edge dislocations in n-type wurtzite GaN. *J. Appl. Phys.* **99**, 033706 (2006).
6. Miller, N. et al. Effect of charged dislocation scattering on electrical and electrothermal transport in n-type InN. *Phys. Rev. B* **84**, 075315 (2011).
7. Look, D. C. & Sizelove, J. R. Dislocation scattering in GaN. *Phys. Rev. Lett.* **82**, 1237 (1999).
8. Amit, V., Adam, P. K., Cain, T. A., Stemmer, S. & Jena, D. Intrinsic mobility limiting mechanisms in lanthanum-doped strontium titanate. *Phys. Rev. Lett.* **112**, 216601 (2014).
9. Mun, H. et al. Large effects of dislocations on high mobility of epitaxial perovskite $Ba_{0.96}La_{0.04}SnO_3$ films. *Appl. Phys. Lett.* **102**, 252105 (2013).
10. Ismail-Beigi, S., Walker, F. J., Cheong, S.-W., Rabe, K. M. & Ahn, C. H. Alkaline earth stannates: the next silicon? *APL Mater.* **3**, 062510 (2015).
11. Kim, H. J. et al. High mobility in a stable transparent perovskite oxide. *Appl. Phys. Express* **5**, 061102 (2012).
12. Niedermeier, C. A. et al. Electron effective mass and mobility limits in degenerate perovskite stannate $BaSnO_3$. *Phys. Rev. B* **95**, 161202 (2017).
13. Raghavan, S. et al. High-mobility $BaSnO_3$ grown by oxide molecular beam epitaxy. *APL Mater.* **4**, 016106 (2016).
14. Wadekar, P. V. et al. Improved electrical mobility in highly epitaxial La:$BaSnO_3$ films on $SmScO_3$(110) substrates. *Appl. Phys. Lett.* **105**, 052104 (2014).

15. Lebens-Higgins, Z. et al. Direct observation of electrostatically driven band gap renormalization in a degenerate perovskite transparent conducting oxide. *Phys. Rev. Lett.* **116**, 027602 (2016).

16. Lee, W.-J. et al. Enhanced electron mobility in epitaxial (Ba,La)SnO₃ films on BaSnO₃(001) substrates. *Appl. Phys. Lett.* **108**, 082105 (2016).

17. Prakash, A. et al. Wide bandgap BaSnO₃ films with room temperature conductivity exceeding 104 S cm⁻¹. *Nat. Commun.* **8**, 15167 (2017).

18. Shiogai, J., Nishihara, K., Sato, K. & Tsukazaki, A. Improvement of electron mobility in La:BaSnO₃ thin films by insertion of an atomically flat insulating (Sr, Ba)SnO₃ buffer layer. *AIP Adv.* **6**, 065305 (2016).

19. Shin, J., Kim, Y. M., Kim, Y., Park, C. & Char, K. High mobility BaSnO₃ films and field effect transistors on non-perovskite MgO substrate. *Appl. Phys. Lett.* **109**, 262102 (2016).

20. Zhang, Z. et al. Evolution of metallicity in vanadium dioxide by creation of oxygen vacancies. *Phys. Rev. Appl.* **7**, 034008 (2017).

21. Yu, S., Yoon, D. & Son, J. Enhancing electron mobility in La-doped BaSnO₃ thin films by thermal strain to annihilate extended defects. *Appl. Phys. Lett.* **108**, 262101 (2016).

22. Ganguly, K. et al. Structure and transport in high pressure oxygen sputter-deposited BaSnO₃₋δ. *APL Mater.* **3**, 062509 (2015).

23. Zhao, C. W., Luo, B. C. & Chen, C. L. Photoconductivity of CaH₂-reduced BaSnO₃ thin films. *RSC Adv.* **7**, 19492–19496 (2017).

24. Scanlon, D. O. Defect engineering of BaSnO₃ for high-performance transparent conducting oxide applications. *Phys. Rev. B* **87**, 161201 (2013).

25. Alagdal, I. A. & West, A. R. Oxygen stoichiometry, conductivity and gas sensing properties of BaSnO₃. *J. Mater. Chem. C.* **4**, 4770–4777 (2016).

26. Ding, L., Nicolay, S., Steinhauser, J., Kroll, U. & Ballif, C. Relaxing the conductivity/transparency trade-off in MOCVD ZnO thin films by hydrogen plasma. *Adv. Funct. Mater.* **23**, 5177–5182 (2013).

27. Oh, C., Heo, S., Jang, H. M. & Son, J. Correlated memory resistor in epitaxial NdNiO₃ heterostructures with asymmetrical proton concentration. *Appl. Phys. Lett.* **108**, 122106 (2016).

28. Lee, W.-J. et al. Oxygen diffusion process in a Ba₀.₉₆La₀.₀₄SnO₃ thin film on SrTiO₃(001) substrate as investigated by time-dependent Hall effect measurements. *Phys. Stat. Sol. (a)* **212**, 1487–1493 (2015).

29. Janotti, A., Varley, J. B., Choi, M. & van de Walle, C. G. Vacancies and small polarons in SrTiO₃. *Phys. Rev. B* **90**, 085202 (2014).

30. Barchuk, M. et al. X-ray diffuse scattering from threading dislocations in epitaxial GaN layers. *J. Appl. Phys.* **108**, 043521 (2010).

31. Heying, B. et al. Role of threading dislocation structure on the x-ray diffraction peak widths in epitaxial GaN films. *Appl. Phys. Lett.* **68**, 643–645 (1996).

32. Kopp, V. S. et al. X-ray determination of threading dislocation densities in GaN-Al₂O₃(0001) films grown by metalorganic vapor phase epitaxy. *J. Appl. Phys.* **115**, 073507 (2014).

33. Kaganer, V. M., Kohler, R., Schmidbauer, M., Opitz, R. & Jenichen, B. X-ray diffraction peaks due to misfit dislocations in heteroepitaxial structures. *Phys. Rev. B* **55**, 1793 (1997).

34. Hino, T. et al. Characterization of threading dislocations in GaN epitaxial layers. *Appl. Phys. Lett.* **76**, 3421–3423 (2000).

35. Nes, E. Recovery revisited. *Acta Metall. Mater.* **43**, 2189–2207 (1995).

36. Lu, G. & Kaxiras, E. Can vacancies lubricate dislocation motion in aluminum? *Phys. Rev. Lett.* **89**, 105501 (2002).

37. Terai, K. et al. In-plane lattice constant tuning of an oxide substrate with Ba₁₋ₓSrₓTiO₃ and BaTiO₃ buffer layers. *Appl. Phys. Lett.* **80**, 4437–4439 (2002).

38. Kim, H. J. et al. Physical properties of transparent perovskite oxides (Ba,La)SnO₃ with high electrical mobility at room temperature. *Phys. Rev. B* **86**, 165205 (2012).